Proceedings of the Seventh International Conference on
Railway Technology: Research, Development and Maintenance
Edited by: J. Pombo
Civil-Comp Conferences, Volume 15, Paper 17.11
Civil-Comp Press, Edinburgh, United Kingdom, 2026
ISSN: 2753-3239, doi: 10.4203/ccc.15.17.11

Low-Power Edge Processing of MFC Sensor Signals for Wayside Railway Monitoring

P. Hadraba[1], R. Krcek[1], J. Chalupa[1], M. Hruzikova[2], F. Kšica[1] and Z. Hadas[1]

[1] Faculty of Mechanical Engineering, Brno University of Technology, Czech Republic
[2] Faculty of Cvil Engineering, Brno University of Technology, Czechia

Abstract

This paper presents a low-power edge measurement node for rail-mounted Macro Fiber Composite (MFC) sensing in railway wayside monitoring. The system acquires train-passage responses directly at the rail, performs local passage detection, axle localization, vehicle-context extraction and anomaly indication, and reports compact diagnostic payloads instead of complete high-rate waveforms. The paper discusses the coupled vehicle–track interpretation of the measured signal, compares charge-amplifier and current-converter readout of the MFC sensor, and demonstrates event-based edge processing on field data. The results show that passage-level and bogie-level descriptors can be extracted locally, reducing communication requirements while preserving information relevant to both infrastructure monitoring and vehicle running gear assessment.

Keywords: wayside railway monitoring, edge computing, macro fiber composite sensor, vehicle-track interaction, low-power sensing, axle detection, anomaly indication

1 Introduction

Efficient sensing systems are inherently selective. Biological nervous systems achieve high computational efficiency by filtering, encoding and partly interpreting sensory information close to the source rather than transmitting all raw stimuli unchanged to higher centres [1]. A comparable principle is used in event-based vision, where bio-inspired sensors transmit asynchronous brightness-change events instead of complete image frames acquired at a fixed rate [2]. This event-oriented view is directly relevant to autonomous railway wayside monitoring. A rail-mounted sensor is excited by every passing wheelset and can generate high-rate time-series data during each train passage, although most passages represent repetitive normal operation.

Railway monitoring approaches can be broadly divided into vehicle-based,wayside systems and infrastructure-based. Dedicated diagnostic vehicles and track-recording cars provide high-quality measurements of track geometry, rail profile and selected defect indicators, but they are periodic by nature and do not observe every regular train passage [3, 4]. On-board monitoring systems can cover long track sections more frequently, but their response is strongly influenced by the vehicle carrying the sensors and by vehicle–track dynamics [4]. In contrast, wayside systems are fixed to the infrastructure and observe many different vehicles at the same location, which makes them suitable for local long-term monitoring of critical track sections [5, 6].

Existing wayside solutions address both vehicle-related tasks, such as wheel-impact or wheel-flat detection, and infrastructure-related tasks using strain gauges, accelerometers, optical fibres or other track-mounted sensors [5–8]. These studies show that local measurements can contain information about both sides of the wheel–rail interface. However, many systems rely on relatively complex installations, multi-sensor arrangements, high data-rate acquisition or backend-centred post-processing of recorded waveforms. The present work builds on previous research of the authors' team on autonomous railway sensing, including energy harvesting for railway wireless sensor nodes, smart sensing systems and rail sensing using piezoelectric elements [9–11]. Here, the focus is on rail-mounted Macro Fiber Composite (MFC) sensing combined with local event-based edge processing and compact passage-level reporting.

The proposed concept treats the MFC sensor as a local sensory element and the analogue front-end with the embedded microcontroller as a peripheral processing layer. The edge node detects train passages, identifies axle-level events, estimates operational parameters and extracts compact diagnostic descriptors related to both local infrastructure response and vehicle running gear behaviour. The measured signal is therefore interpreted as a local response of the coupled vehicle–track system, not as an infrastructure-only measurement.

The architecture is positioned as a low-power edge front-end within an edge–cloud hierarchy, not as a replacement for diagnostic vehicles, detailed inspection methods or cloud-based railway diagnostics. The edge node performs the first stage of interpretation, while the backend is used for visualization, cross-passage comparison and degradation modelling. This partitioning is important because a purely cloudcentred architecture would require repeated transmission of complete raw waveforms from train passages. Edge computing reduces bandwidth demand, response time and battery-related constraints by shifting computation closer to the data source [12]. In wireless sensor networks, low-power nodes are expected to deliver information at low data rates [13], and radio transmission is often more energy-demanding than local sensing or computation [14]. Repeated normal passages should therefore be represented by compact passage-level and axle-level descriptors, with raw records reserved for selected events, calibration and algorithm development.

A key distinction of the proposed approach is that the measured MFC signal is treated as a mixed response containing both the excitation generated by the passing vehicle and the transfer behaviour of the local track structure. Vehicle context is therefore included in the processing chain. Grouping passages by axle arrangement, estimated speed and probable vehicle type makes it possible to compare similar passages over time and to distinguish repeated local infrastructure effects from anomalies tied to a particular vehicle, bogie or axle group.

The contribution of this paper is demonstrated on a functional low-power measurement unit for rail-mounted MFC sensing. The unit performs local edge processing to detect train passages, identify axle-related events, estimate operating context, support vehicle-type classification and flag signal-level anomalies. The resulting compact payload is reported to a higher-level system. At this stage, the system is considered an edge front-end for passage characterization and anomaly indication; confirmed defect classification, fault attribution and long-term degradation prediction remain backend-level tasks for further work.

2 Wayside Monitoring and Edge Processing of Vehicle–Track Interaction

A rail-mounted MFC sensor does not measure the condition of the rail or the vehicle independently. It measures the local structural response generated by the wheel—rail interaction. During each train passage, the moving wheel loads excite the rail, fasteners, sleepers and supporting track structure. The measured signal is therefore a coupled signature containing both vehicle-related effects and infrastructure-related effects. Vehicle-related contributions are associated mainly with axle arrangement, bogie configuration, wheel condition, speed and loading. Infrastructure-related contributions are associated with local track stiffness, support conditions, rail discontinuities and gradual changes of the monitored section.

2.1 Measurement Concept and Node Architecture

The proposed monitoring concept is implemented as a low-power measurement node installed directly at the rail. The signal chain consists of the bonded MFC sensor, analogue signal conditioning, analogue-to-digital conversion, an embedded microcontroller, local edge processing and a communication interface to the higher-level system.

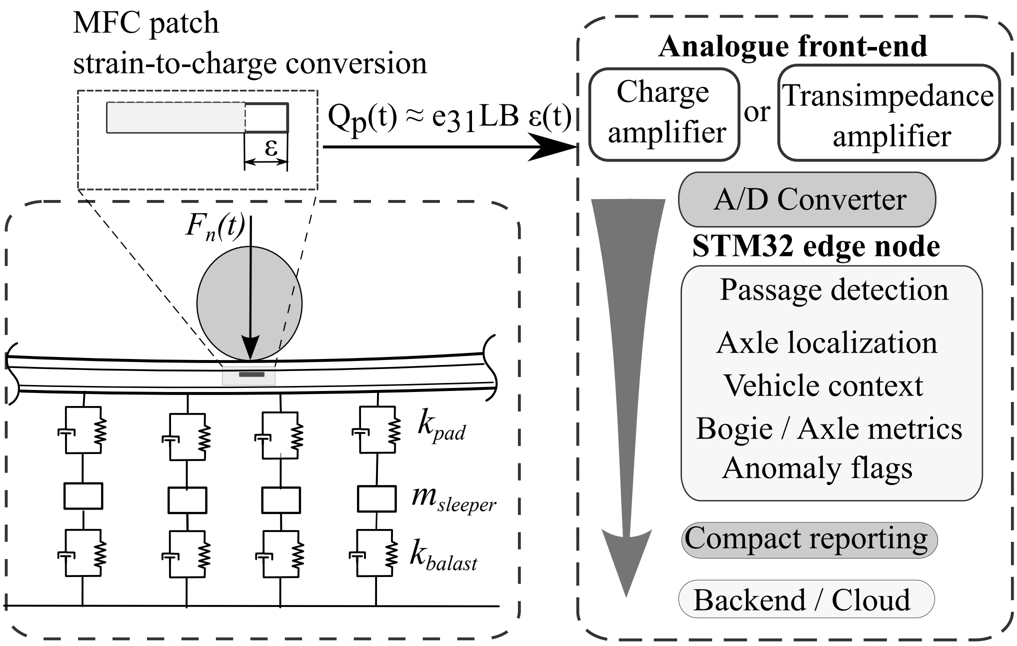

Figure 1: Schematic architecture of rail-mounted MFC wayside monitoring: from mechanical wheel–rail excitation and MFC electromechanical coupling to embedded edge processing and compact reporting.

Figure 1 summarizes the measurement and processing concept. The passing wheel excites the rail through the wheel–rail contact force, while the local track structure transfers this excitation to rail deformation at the sensor location. The bonded MFC patch converts the deformation-related response into an electrical signal, which is conditioned by the analogue front-end and processed by the STM32 edge node. The purpose of the system is to transform each passage into a compact diagnostic record containing operational context, axle or bogie descriptors, anomaly flags and selected trend-relevant quantities.

The architecture is designed for autonomous field operation. Each additional sensing channel increases analogue complexity, ADC usage, memory requirements and energy consumption. The processing chain is therefore designed to extract as much information as possible from a minimal number of rail-mounted sensing channels.

2.2 Signal Content During a Train Passage

The signal generated during a train passage contains several levels of information. The timing of individual response peaks is associated with axle positions and can be used to estimate axle count, axle spacing and train speed. The low-frequency part of the signal describes the slower deformation response of the monitored track section and is useful for passage segmentation, axle localization and comparison of similar train passages. The high-frequency part contains fast local transients and impulse-like components, which are more sensitive to abnormal wheel–rail interaction and localised dynamic events.

This division is important for both hardware and algorithm design. A signal representation suitable for robust passage detection is not necessarily the most sensitive representation for detecting short high-frequency impacts. The measurement chain must therefore be selected with respect to the diagnostic objective, available power budget and required robustness of the field deployment.

2.3 MFC Sensor Readout

A key design choice is the analogue readout of the MFC sensor. The MFC sensor bonded to the rail is treated as a piezoelectric strain sensor. In a simplified one-dimensional form, assuming approximately uniform longitudinal strain over the active electrode area, the mechanically generated charge can be written as

$$Q_p(t) \approx e_{31} LB \cdot \varepsilon_s(t), \tag{1}$$

where $Q_p(t)$ is the generated charge, $\varepsilon_s(t)$ is the longitudinal rail strain averaged over the active area of the MFC patch, e_{31} is the effective piezoelectric stress coefficient in the sensing direction, and L and B are the length and width of the active electrode area. In practical rail-mounted measurements, this relation is affected by sensor orientation, bonding quality and non-uniform strain distribution under the patch, but it provides a useful first-order description of the sensor output.

Charge-Amplifier Readout If the sensor is connected to a charge amplifier with feedback capacitance C_f, the output voltage is proportional to the generated charge and therefore to the deformation-related response of the rail:

$$V_Q(t) - V_{\text{ref}} \approx -\frac{Q_p(t)}{C_f} \approx -\frac{e_{31} LB}{C_f} \cdot \varepsilon_s(t). \tag{2}$$

The charge-amplifier configuration is suitable for robust passage detection, axle localization and extraction of the low-frequency passage envelope. It also avoids numerical integration of the measured signal, which is advantageous for embedded processing because integration is sensitive to offsets, drift and finite record length.

Current-Converter Readout In contrast, a current converter measures the piezoelectric current, which is the time derivative of the generated charge:

$$I_p(t) = \frac{\mathrm{d}Q_p(t)}{\mathrm{d}t} \approx e_{31} LB \cdot \dot{\varepsilon}_s(t). \tag{3}$$

For a transimpedance current converter with feedback resistance R_T, the output voltage is proportional to the strain-rate-related response:

$$V_I(t) - V_{\text{ref}} \approx -R_T I_p(t) \approx -R_T e_{31} LB \cdot \dot{\varepsilon}_s(t). \tag{4}$$

This readout emphasizes rapid changes in rail deformation and increases the relative importance of higher-frequency components. It can therefore be useful for short impulsive events and local wheel–rail impacts, while the charge-amplifier path is more suitable for robust autonomous passage processing.

2.4 Power Consumption

Power consumption is a key constraint for autonomous wayside deployment. The node is operated as an event-based system: most of the time it remains in a low-power state, and the energy-demanding processing and radio transmission phases are activated only after a train passage has been detected. The measured operating states are summarized in Table 1.

Table 1: Measured power consumption of the edge measurement node in individual operating states.

State	**Current draw**	**Duration**	**Description**
Sleep	$150\ \mu\mathrm{A}$	continuous	Low-power state between train passages
Processing	$12\ \mathrm{mA}$	$3\ \mathrm{s}$	Local signal analysis on the microcontroller
Reporting	$33\ \mathrm{mA}$	$3\ \mathrm{s}$	LoRa transmission of the compact payload

For an example operating scenario of 104 reported events per day, the average current draw was estimated as approximately $0.31\ \mathrm{mA}$, corresponding to a theoretical minimum capacity of about $272\ \mathrm{mAh}$ for 30 days without energy harvesting. This value represents only a lower bound for the measurement electronics and does not include practical reserves for converter losses, temperature effects, ageing or increased communication activity.

A more robust supply configuration, previously verified in field deployments for energy-demanding operation including transmission of complete measurement records, uses a $12.8\ \mathrm{V}$, $100\ \mathrm{Ah}$ $LiFePO_4$ battery with a $100\ \mathrm{W_p}$ photovoltaic panel. Since the proposed edge-processing node transmits compact reports instead of complete waveforms, its optimal supply configuration will likely lie between the theoretical minimum and this robust solar-assisted setup. The same electronics can therefore be scaled from a low-cost battery-powered installation for low-traffic lines to a more resilient autonomous unit for densely operated corridors.

2.5 Event-Based Edge Processing and Compact Reporting

The embedded processing chain is organized around train passages as discrete events. Once a passage is detected, the relevant signal segment is acquired and processed locally. The processing sequence includes offset removal, filtering, passage segmentation, axle-event detection, speed estimation, metric extraction and anomaly indication.

The output of the node is a compact diagnostic payload rather than a complete high-rate time series. In the implemented LoRaWAN reporting scheme, the passage report is encoded as a fixed binary frame of $46\ \mathrm{B}$, summarized in Table 2.

Table 2: Compact LoRaWAN passage-report payload used by the edge node.

Block	**Size [B]**	**Type**	**Content**
Global status	8	fixed	node flags, battery voltage and environmental quantities
Channel 0	19	fixed	train index, estimated speed, number of bogies and bogie-level anomaly masks
Channel 1	19	fixed	same descriptor set for the second sensing channel
Total	46	fixed	binary LoRaWAN telemetry frame

The fixed-size frame avoids transmitting raw waveforms or variable-length text fields. Vehicle names are reconstructed in the backend from the transmitted train index, while bogie-level anomaly positions are represented by bit masks. With the evaluated EU868 LoRaWAN settings, the $46\ \mathrm{B}$ payload gives a packet time-on-air of approximately $288\ \mathrm{ms}$, which was used in the power and reporting-rate estimate.

The backend acts as a supervisory and long-term analysis layer. It stores compact passage records, groups comparable passages, visualizes operating history and supports long-term trend evaluation. The measurement node therefore serves as an edge front-end: it performs local event detection and data reduction, while confirmed diagnostic interpretation remains a backend-level task.

3 Vehicle Context and Signal-Level Anomaly Indicators

3.1 Vehicle Identification as Operational Context

Vehicle identification provides the operational context required for interpreting the measured MFC response. The same local track section can produce different signal amplitudes and frequency content depending on the passing vehicle, axle arrangement, speed and loading. For this reason, each detected passage is assigned a vehicle-context descriptor derived from axle timing and comparison with an internal rolling-stock database.

The preferred way to estimate train speed in a wayside setup is to use two spatially separated sensing channels. If the distance Δx_s between the channels is known, the speed can be obtained directly from the time delay Δt_s between corresponding axle events,

$$v \approx \frac{\Delta x_s}{\Delta t_s}. \tag{5}$$

This method does not require prior knowledge of the vehicle geometry and is therefore preferred for accurate speed estimation. However, the proposed architecture also supports a database-based fallback when one channel is unavailable, degraded or intentionally omitted in a minimal low-power configuration.

In the fallback mode, the vehicle candidate is not identified from absolute axle distances. Instead, the edge node first uses the relative axle-timing pattern measured within a single passage. For approximately constant speed during the passage, the ratio of two measured axle-time intervals is equal to the ratio of the corresponding axle distances,

$$r_{ij} = \frac{\Delta t_{ij}}{\Delta t_{\mathrm{ref}}} \approx \frac{\Delta x_{ij}}{\Delta x_{\mathrm{ref}}}, \tag{6}$$

where Δt_{ij} is the measured time interval between selected axle-related events and Δt_{ref} is a reference interval from the same passage. The speed term cancels in this ratio, so the measured pattern can be compared with dimensionless axle-spacing ratios stored in the rolling-stock database before the absolute speed is known.

After a probable vehicle candidate has been assigned, its known absolute axle or bogie-feature distance Δx_{ij} can be combined with the measured time interval Δt_{ij} to estimate speed,

$$v \approx \frac{\Delta x_{ij}}{\Delta t_{ij}}. \tag{7}$$

The database-based estimate is therefore a two-step fallback procedure: first, a vehicle candidate is selected using speed-independent axle ratios; second, the known absolute geometry of that candidate is used to estimate speed. The method is less general than direct two-channel timing because it depends on correct vehicle identification, but it preserves approximate speed estimation when direct speed measurement is not available.

Vehicle context is also necessary for anomaly interpretation. Without knowledge of the expected axle arrangement and passage structure, normal differences between vehicle types could be misinterpreted as abnormal wheel–rail contact behaviour. Grouping comparable passages by vehicle type, axle arrangement and speed therefore provides the basis for separating vehicle-dependent variability from signal-level anomalies.

3.2 Bogie-Level Anomaly Indicator

The anomaly indicator is based on relative comparison within a single train passage rather than on a universal reference spectrum. This choice reduces the influence of site-specific factors such as local track structure, sensor installation, analogue front-end, speed and loading conditions. The passage is segmented into bogie-level windows and each bogie is compared with the remaining bogies of the same train.

For each bogie segment, a localized spectral analysis is performed. The segment is detrended, windowed and transformed into the frequency domain. A band-energy indicator is then evaluated as

$$E_b^{(k)} = \int_{f_1}^{f_2} S_b^{(k)}(f)\,\mathrm{d}f, \tag{8}$$

where $S_b^{(k)}(f)$ is the power spectral density of the k-th bogie segment and $[f_1, f_2]$ is the frequency band used for anomaly screening. In the prototype, the band 50–$200\,\mathrm{Hz}$ was used as a practical indicator of increased dynamic activity associated with wheel–rail interaction.

The 50–$200\,\mathrm{Hz}$ range was selected as an empirical screening band for the present MFC setup. It covers the upper part of the dominant coupled vehicle–track response, including the P2 resonance region reported around 30–$100\,\mathrm{Hz}$, and extends into the lower higher-harmonic range where impact-like wheel–rail events increase the spectral energy. In the preparatory data, regular passages showed low energy in this band, whereas candidate anomalous bogie segments produced a clear increase of normalized band energy. The band is therefore used as a robust edge-compatible indicator, not as a universal defect-frequency signature.

To reduce the influence of absolute signal amplitude, the band energy is normalized by the signal level within the same bogie window,

$$\eta_b^{(k)} = \frac{E_b^{(k)}}{\mathrm{RMS}_k^2}. \tag{9}$$

A bogie is treated as a signal-level anomaly candidate if its normalized band energy exceeds a robust threshold derived from the same passage,

$$\eta_b^{(k)} > \mathrm{median}(\boldsymbol{\eta}_b) + \alpha\,\mathrm{MAD}(\boldsymbol{\eta}_b), \tag{10}$$

where $\boldsymbol{\eta}_b$ is the set of normalized band-energy indicators for all bogies in the passage, MAD is the median absolute deviation and α is a tunable threshold.

This criterion does not provide confirmed wheel-defect classification. Increased spectral energy may be caused by wheel flats, polygonal wear, bogie dynamics, axle-load differences, local wheel–rail impacts or infrastructure-related excitation. The indicator is therefore used to select bogies or passages for compact reporting, raw-data retention or subsequent backend analysis.

4 Results and Discussion

The evaluation was carried out in two steps. First, previously recorded passage data from August to December 2025 were used as a development and verification dataset. These records contained complete raw waveforms and therefore allowed the signal-processing chain to be designed, tuned and debugged offline. This stage was used to verify passage detection, axle localization, vehicle-context extraction, speed estimation and the calculation of spectral indicators for anomaly screening. Second, the implemented edge unit was tested in the field. In this configuration, the node operated directly at the rail, acquired the MFC signal, processed train passages locally and transmitted compact passage reports through the LoRa communication interface. The field test therefore verified the complete hardware–software chain from sensing and analogue conditioning to embedded processing and wireless reporting.

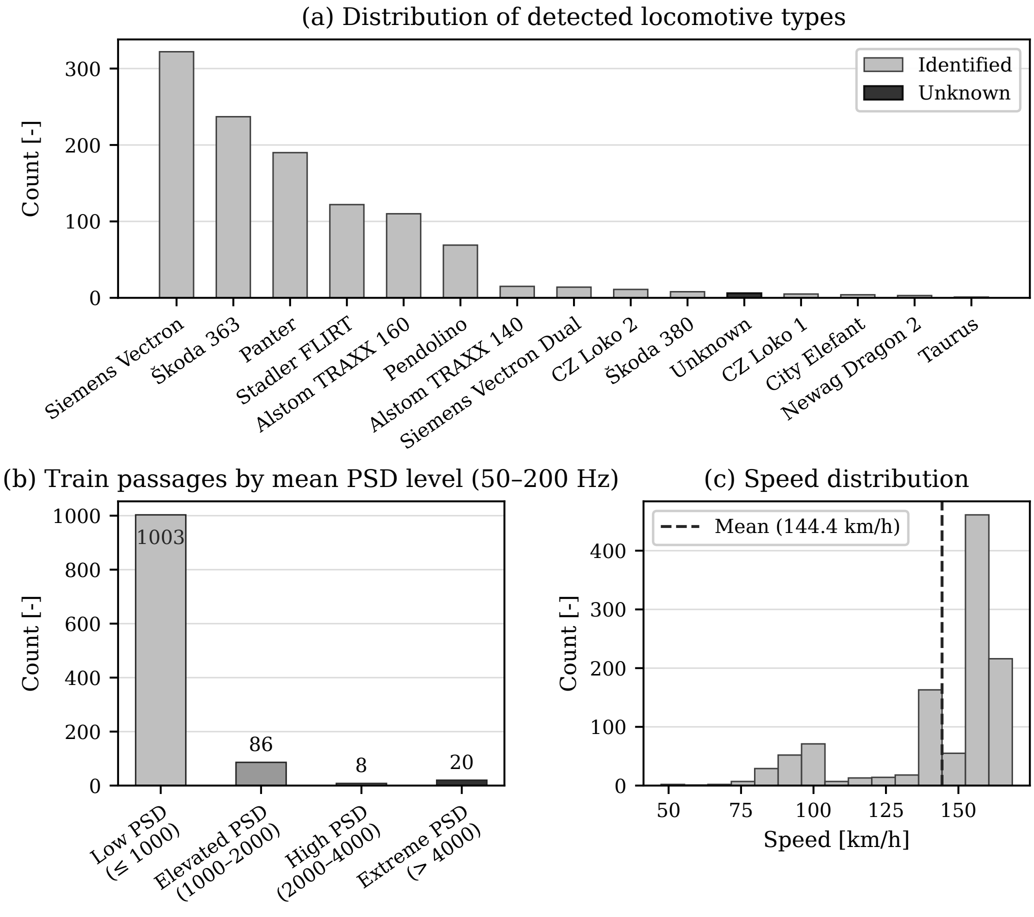

Figure 2: Passage-level processing of the preparatory dataset: (a) distribution of detected traction vehicles or complete train units, (b) categorization according to the mean PSD level in the 50–200 Hz band, and (c) distribution of estimated train speeds.

Figure 2 summarizes the passage-level outputs obtained from the preparatory dataset.

Panel (a) shows the distribution of detected traction vehicles or complete train units. This output represents the vehicle-context layer required for comparing similar passages over time. Panel (b) shows the categorization of passages according to the mean power spectral density in the $50–200\,\mathrm{Hz}$ band. This band was used as a practical indicator of increased dynamic activity: a smooth passage is expected to excite mainly the lower-frequency passage response, whereas abnormal wheel–rail interaction, bogie dynamics or impact-like events may increase spectral energy in this range. Panel (c) shows the estimated train speed. The distribution confirms that the monitored section is dominated by high-speed operation, with most passages concentrated close to $160\,\mathrm{km\,h^{-1}}$.

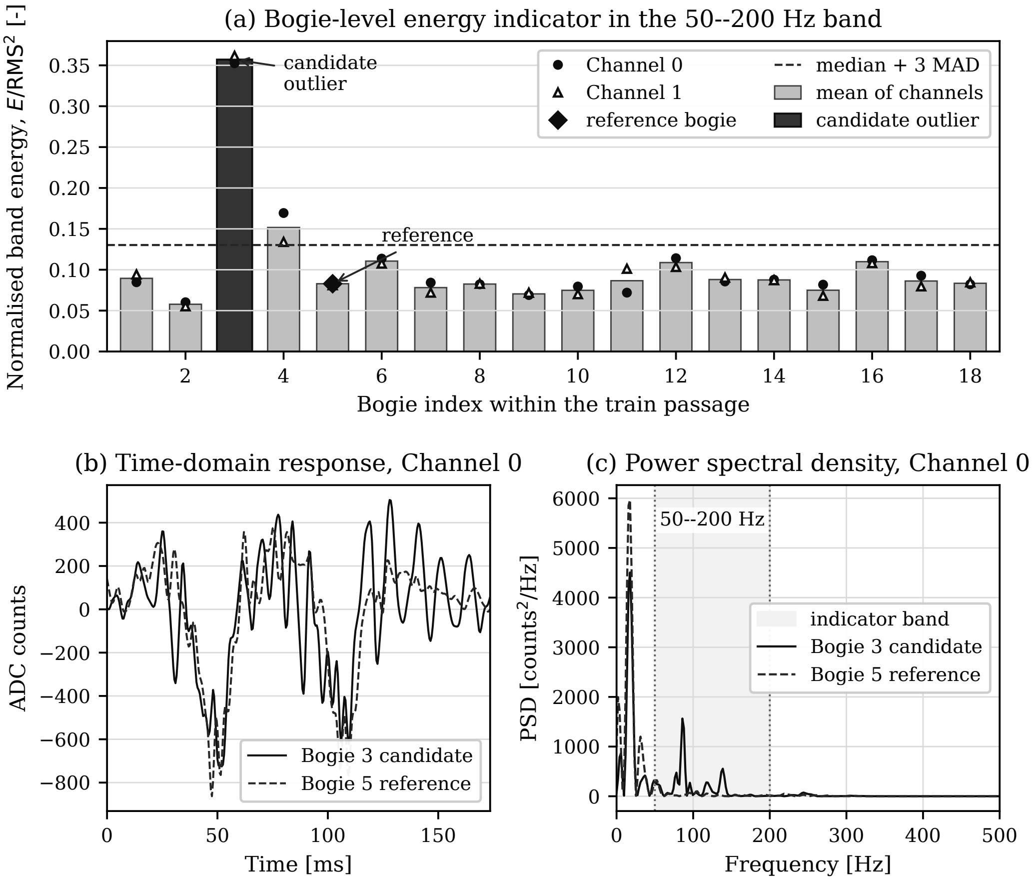

Figure 3: Bogie-level anomaly indication within a single train passage. Panel (a) shows the normalised band-energy indicator for all bogies, with the outlier candidate and reference bogie highlighted. Panels (b) and (c) compare their time-domain response and power spectral density; the shaded band marks the frequency range used for the indicator. The result represents signal-level anomaly screening, not confirmed wheel-defect classification.

The passage-level statistics demonstrate that the edge-processing chain can extract operational context and diagnostic screening indicators from a large set of raw waveforms. However, passage-level descriptors alone do not show how a specific anomaly candidate is localized within a train. For this reason, Figure 3 presents a detailed example of bogie-level anomaly indication within a single passage.

In this example, the relative comparison of bogie-level indicators identifies an abnormal response near the beginning of the train, corresponding to a bogie of the first vehicle behind the Vectron locomotive. Panel (a) shows the normalized band-energy indicator for individual bogies within the same train passage. The highlighted bogie exceeds the robust threshold and is therefore treated as a signal-level outlier candidate, while another bogie from the same passage is used as a reference. Panel (b) compares the corresponding time-domain responses and shows visibly stronger dynamic components in the candidate segment. Panel (c) compares the power spectral densities and shows increased spectral energy in the selected $50–200\,\mathrm{Hz}$ band, which forms the basis of the implemented anomaly indicator.

The combined offline and field evaluation confirms the intended role of the proposed system. The node is not only a data logger, but a local edge-processing front-end capable of converting high-rate MFC waveforms into compact train-passage reports. The offline dataset provided the raw waveform basis for algorithm development, while the field test verified autonomous operation and LoRa-based reporting under real trackside conditions. At the present stage, the system is functional both from the hardware and software perspective and can autonomously evaluate train passages at the measurement site.

The main remaining limitation is the diagnostic validation layer. The indicators presented in Figures 2 and 3 quantify signal-level differences, but they do not provide confirmed classification of defect types. Increased spectral energy may be caused by wheel flats, polygonal wear, bogie dynamics, axle-load differences, local wheel–rail impacts or infrastructure-related excitation. Reliable attribution of anomalies to specific vehicle or infrastructure faults therefore requires larger labelled datasets and comparison with maintenance or service records. Future work will focus mainly on improving fault classification, validating anomaly indicators against confirmed defects and extending long-term trend analysis.

5 Conclusion

This work demonstrated a functional low-power edge measurement unit for rail-mounted MFC sensing in wayside railway monitoring. The unit acquires train-passage responses, detects axle-related events, estimates passage parameters, supports vehicle-context extraction and transmits compact reports instead of complete high-rate waveforms. The proposed architecture therefore shifts the first stage of interpretation from the backend to the measurement site.

The evaluation was carried out in two complementary steps. Previously recorded raw waveforms were used for offline development, tuning and verification of the signal-processing chain. A subsequent field test verified the complete hardware–software path, including rail-mounted sensing, analogue conditioning, embedded processing and LoRa-based reporting. These results confirm that a substantial part of passage characterization can be performed directly at the measurement node, which is essential for applications where communication bandwidth, storage capacity and energy consumption are constrained.

The results also show that vehicle context is necessary for meaningful interpretation of the MFC response. The measured signal depends not only on the local track structure, but also on the axle arrangement, speed, loading and running-gear condition of the passing vehicle. Vehicle identification and axle-pattern analysis therefore provide the operational context required for comparing similar passages, estimating speed and separating normal vehicle-dependent variability from signal-level anomalies.

From the energy perspective, the node can be scaled between two practical deployment modes. For low-traffic lines or short-term validation campaigns, the low average consumption enables compact battery-powered operation. For densely operated corridors or installations requiring long unattended operation, the same edge-processing concept can be combined with a more robust solar-assisted $LiFePO_4$ battery supply. In both cases, local processing reduces the amount of transmitted data and reserves complete waveform transmission for selected events, calibration or further algorithm development.

The presented system should be interpreted as an edge front-end for passage characterization and anomaly indication, not as a finalized fault-diagnosis system. The main remaining challenge is diagnostic validation: signal-level anomalies must be linked to confirmed wheel, bogie or infrastructure defects using labelled datasets, maintenance records and long-term trend analysis. Future work will therefore focus on improving fault classification, validating anomaly indicators against confirmed defects and extending backend-level comparison of repeated passages from comparable vehicles.

Acknowledgements

This publication was supported by the Technology Agency of the Czech Republic through project No. CL02000086, “Advanced Diagnostics of Railway Turnout Movable Parts”.

References

[1] P. Sterling and S. Laughlin, *Principles of Neural Design*, MIT Press, Cambridge, MA, USA, 2015. doi: 10.7551/mitpress/9780262028707.001.0001.

[2] G. Gallego, T. Delbrück, G. Orchard, C. Bartolozzi, B. Taba, A. Censi, S. Leutenegger, A.J. Davison, J. Conradt, K. Daniilidis and D. Scaramuzza, “Event-Based Vision: A Survey”, *IEEE Transactions on Pattern Analysis and Machine Intelligence*, 44(1), 154–180, 2022. doi: 10.1109/TPAMI.2020.3008413.

[3] A. Farkas, "Measurement of railway track geometry: A state-of-the-art review," *Periodica Polytechnica Transportation Engineering*, vol. 48, no. 1, pp. 76–88, 2020. doi: 10.3311/PPtr.14145.

[4] P. Weston, C. Ling, C. Roberts, C. Goodman, P. Li, and R. Goodall, "Monitoring vertical track irregularity from in-service railway vehicles," *Proceedings of the Institution of Mechanical Engineers, Part F: Journal of Rail and Rapid Transit*, 2015.

[5] G. Kouroussis, C. Caucheteur, D. Kinet, G. Alexandrou, O. Verlinden, and V. Moeyaert, "Review of trackside monitoring solutions: From strain gages to optical fibre sensors," *Sensors*, vol. 15, no. 8, pp. 20115–20139, 2015. doi: 10.3390/s150820115.

[6] A. Mosleh, M. Mohammadi, R. Silva, J. Magalh aes, T. Jorge, C. Vale, D. Ribeiro, and W. Zhai, "Recent advances in wayside condition monitoring for railways: A comprehensive review," *Railway Engineering Science*, 2026. doi: 10.1007/s40534-025-00423-2.

[7] W. Fu, Q. He, Q. Feng, J. Li, F. Zheng, and B. Zhang, "Recent advances in wayside railway wheel flat detection techniques: A review," *Sensors*, vol. 23, no. 8, article 3916, 2023. doi: 10.3390/s23083916.

[8] C. Du, S. Dutta, P. Kurup, T. Yu, and X. Wang, "A review of railway infrastructure monitoring using fiber optic sensors," *Sensors and Actuators A: Physical*, vol. 303, article 111728, 2020. doi: 10.1016/j.sna.2019.111728.

[9] Z. Hadaš, O. Rubeš, F. Kšica, and J. Chalupa, "Kinetic electromagnetic energy harvester for railway applications-development and test with wireless sensor," *Sensors*, vol. 22, no. 3, pp. 1–19, 2022. ISSN: 1424-8220.

[10] F. Kšica, O. Rubeš, J. Kovář, J. Chalupa, and Z. Hadaš, "Smart sensing system for railway monitoring," in *Proceedings of the 2022 20th International Conference on Mechatronics – Mechatronika (ME)*, Pilsen: IEEE, 2022, pp. 1–6. ISBN: 978-1-6654-1040-3.

[11] Z. Machů, M. Kratochvílová, F. Kšica, J. Podroužek, and Z. Hadaš, "Sensing rail system with piezoelectric elements," *MM Science Journal*, no. March 2021, pp. 4230–4237, 2021. ISSN: 1805-0476.

[12] W. Shi, J. Cao, Q. Zhang, Y. Li and L. Xu, "Edge Computing: Vision and Challenges", *IEEE Internet of Things Journal*, 3(5), 637–646, 2016. doi: 10.1109/JIOT.2016.2579198.

[13] G.J. Pottie and W.J. Kaiser, "Wireless Integrated Network Sensors", *Communications of the ACM*, 43(5), 51–58, 2000. doi: 10.1145/332833.332838.

[14] J. Krawiec, M. Wybraniak-Kujawa, I. Jacyna-Gołda, P. Kotylak, A. Panek, R. Wojtachnik and T. Siedlecka-Wójcikowska, "Energy Footprint and Reliability of IoT Communication Protocols for Remote Sensor Networks", *Sensors*, 25(19), 6042, 2025. doi: 10.3390/s25196042.